



Improved SARS-CoV-2 M^{pro} inhibitors based on feline antiviral drug GC376: Structural enhancements, increased solubility, and micellar studies

Wayne Vuong^a, Conrad Fischer^{a,1}, Muhammad Bashir Khan^b, Marco J. van Belkum^a, Tess Lamer^a, Kurtis D. Willoughby^a, Jimmy Lu^{b,d}, Elena Arutyunova^{b,d}, Michael A. Joyce^{c,d}, Holly A. Saffran^{c,d}, Justin A. Shields^{c,d}, Howard S. Young^b, James A. Nieman^{c,e}, D. Lorne Tyrrell^{c,d}, M. Joanne Lemieux^{b,d}, John C. Vederas^{a,*}

^a Department of Chemistry, University of Alberta, Edmonton AB, T6G 2G2, Canada

^b Department of Biochemistry, Membrane Protein Disease Research Group, University of Alberta, Edmonton AB, T6G 2R3, Canada

^c Department of Medical Microbiology and Immunology, University of Alberta, Edmonton AB, T6G 2R3, Canada

^d Li Ka Shing Institute of Virology, University of Alberta, Edmonton AB, T6G 2E1, Canada

^e Li Ka Shing Applied Virology Institute, University of Alberta, Edmonton AB, T6G 2E1, Canada

ARTICLE INFO

Article history:

Received 15 March 2021

Received in revised form

3 May 2021

Accepted 22 May 2021

Available online 30 May 2021

Keywords:

COVID-19

Main protease

Protease inhibitor

Crystallography

Structure-guided design

GC376 analogs

ABSTRACT

Replication of SARS-CoV-2, the coronavirus causing COVID-19, requires a main protease (M^{pro}) to cleave viral proteins. Consequently, M^{pro} is a target for antiviral agents. We and others previously demonstrated that GC376, a bisulfite prodrug with efficacy as an anti-coronaviral agent in animals, is an effective inhibitor of M^{pro} in SARS-CoV-2. Here, we report structure-activity studies of improved GC376 derivatives with nanomolar affinities and therapeutic indices >200. Crystallographic structures of inhibitor-M^{pro} complexes reveal that an alternative binding pocket in M^{pro}, S4, accommodates the P3 position. Alternative binding is induced by polar P3 groups or a nearby methyl. NMR and solubility studies with GC376 show that it exists as a mixture of stereoisomers and forms colloids in aqueous media at higher concentrations, a property not previously reported. Replacement of its Na⁺ counter ion with choline greatly increases solubility. The physical, biochemical, crystallographic, and cellular data reveal new avenues for M^{pro} inhibitor design.

© 2021 Elsevier Masson SAS. All rights reserved.

1. Introduction

The end of 2019 saw the beginnings of what would quickly become a global pandemic in the form of COVID-19 (coronavirus disease 2019), caused by severe acute respiratory syndrome coronavirus 2 (SARS-CoV-2). Bearing a high degree of genetic similarity to SARS-CoV that was responsible for an outbreak in 2002–2004 [1,2], it has developed into a widespread disease with >70 million cases and >1.6 million deaths worldwide as of December 2020, with numbers continuing to rise [3]. Due to the success of public health measures in containing SARS-CoV, development of anti-

SARS therapeutics was discontinued. Consequently, there is an urgent need for anti-viral drug development for acute COVID-19 patients. Furthermore, in spite of vaccines being deployed for use, current information regarding the duration of immunity, effectiveness against mutant strains as well as possibility of reinfection remains limited.

SARS-CoV and SARS-CoV-2 are positive strand RNA viruses that exploit host cellular machinery to translate genetic information into viral proteins required for replication. As part of this process, two overlapping polyproteins are encoded: pp1a and pp1ab, which are then cleaved into the individual active proteins necessary for viral transcription and replication [4]. Two proteases are responsible for executing these vital steps: M^{pro} (also called 3CL^{pro}) and a papain like protease (PL^{pro}) that cleave 11 and 3 times, respectively. The 11 proteolytic cleavage sites of M^{pro} are usually at conserved Leu Gln | Ser Ala Gly sequences. Due to the critical role of this

* Corresponding author.

E-mail address: john.vederas@ualberta.ca (J.C. Vederas).

¹ Present address: Department of Physical Sciences, Barry University, 11300 NE 2nd Ave., Miami Shores FL 33161, USA.

enzyme in viral replication, M^{pro} is an attractive target for antiviral agents [5,6]. M^{pro} is a cysteine protease, a class of enzymes for which a large variety of inhibitors exist [7,8].

Potent M^{pro} inhibitors may be viable drugs if certain criteria are fulfilled, namely good bioavailability, low toxicity and ample solubility [8]. As a result of these requirements, a number of seemingly promising cysteine protease inhibitors have failed when examined as possible drug candidates. A prominent example of this is rupintrivir, targeted as a treatment for rhinoviruses [9]. As an unsaturated ester Michael acceptor, it exhibited low bioavailability in clinical trials [10], probably partly due to the irreversible nature of the covalent bond formed upon attack by sulfur nucleophiles. This lack of reversibility can result in permanent off-target binding to other thiol-containing biomolecules present in mammalian cells, leading to destruction or sequestration of the inhibitor. Additionally, off-target binding to untargeted thiols could lead to toxicity or host immune response [8]. Hence, inhibitors possessing warheads that bind reversibly and preferentially to the target cysteine protease are desirable. Peptide aldehydes present an attractive solution as they are able to bind reversibly to thiol-containing target molecules, forming a hemithioacetal in the process [11,12]. In addition, they can be readily derivatized to more water-soluble bisulfite adducts for administration as prodrugs [13]. Subsequent reversion of the bisulfite adduct to the parent aldehyde under physiological conditions then restores the active form of the inhibitor [6].

Early studies by Wolfenden and coworkers on peptide aldehydes as protease inhibitors [11], prompted us to examine them as potent inhibitors of viral cysteine proteases [12]. In 2016, Kim et al. discovered GC376 as a drug active against the feline coronavirus (FCoV) responsible for feline infectious peritonitis (FIP) [14]. GC376 is a bisulfite adduct prodrug of the corresponding parent aldehyde, GC373, which strongly inhibits the M^{pro} of FCoV. The effectiveness of this compound was demonstrated when cats exhibiting FIP were cured upon administration of this drug [14]. Once symptoms are present, untreated FIP has close to a one hundred percent fatality rate in cats. The utility of this drug is made more remarkable due to the well-tolerated nature of GC376. Further studies have demonstrated its activity against the M^{pro} of a number of other coronaviruses, including those of minks and ferrets [14–16]. Recently, we showed that GC376 and GC373 were also potent inhibitors of the SARS-CoV-2 M^{pro} and that these drugs were able to block virus replication in cell culture, indicating that they are good candidates as antivirals for the treatment of COVID-19 [6]. Independently, different groups published similar observations [17–22], with further follow-up studies subsequently demonstrating efficacy in transgenic mouse models, strongly supporting the translational potential of GC376 and related analogs for human use [23–25]. Additionally, we also experimentally demonstrated the reversible nature of GC376 [26]. During 2020, a number of promising potent reversible inhibitors of SARS-CoV-2 M^{pro} have been uncovered, including α -ketoamides [2], and α -hydroxymethyl and α -acyloxymethylketones [27].

We now report efforts to increase the effectiveness of GC376 analogs against SARS-CoV-2. Improvements by modification of the chemical structure of GC376 resulted in a number of compounds with improved binding characteristics and nanomolar inhibition of SARS-CoV-2 M^{pro} . The structure-activity relationship (SAR) study was accomplished with systematic optimization of inhibitor structures via detailed assessments of these new compounds co-crystallized with SARS-CoV-2 M^{pro} and subsequent *in vitro* testing with recombinant protease as well as with mammalian cell lines. Furthermore, co-crystallization studies revealed an alternative mode of binding for these new inhibitors compared to GC376, facilitating a better fit into the active site of M^{pro} . NMR studies with

^{13}C -labelled GC373 and GC376 confirm that in aqueous media the former exists as a hydrated aldehyde and is a mixture of stereoisomers due to epimerization at the α -carbon of the glutamine analog. The formation of bisulfite adduct GC376 leads to additional stereoisomers. These spontaneously convert to the aldehyde, and only a single isomer is seen bound to the SARS-CoV-2 M^{pro} enzyme. It was also found that versions of GC376 with alternative cations led to an increase in drug solubility, potentially allowing for smaller volumes during drug administration. Finally, solubility testing and NMR experiments demonstrated the formation of colloidal aggregates by GC376, which may enable administration of small volumes of highly concentrated drug.

2. Results

2.1. Structure guided development of M^{pro} inhibitors using independent variations in P2 and P3

Development of improved inhibitors began with sampling variations in the P2 and P3 sites of GC376 in order to assess which types of combinations would facilitate the greatest increase in binding to M^{pro} (Fig. 1). The cyclic glutamine analog in the P1 site of the inhibitor was maintained due to the numerous favorable interactions of this residue observed with the S1 pocket of M^{pro} , as determined from our previous study [6]. The aldehyde warhead was also conserved due to the ability to easily and favorably form the bisulfite prodrug in a single step, combined with the proven efficacy of this group, as was shown with GC376 to treat FIP in felines [14].

Based on our previous crystal structures, the S2 pocket of SARS-CoV-2 M^{pro} responsible for binding of the leucine moiety in GC376 was largely hydrophobic [6], and so lipophilic variants of the leucine isopropyl group in the P2 site of the inhibitor were chosen such as cyclopropyl (**1a**), cyclohexyl (**1b**), and phenyl (**1c**) (Table 1). Replacement with a phenyl group (**1c**) yielded only moderate improvements in IC_{50} values using a FRET substrate-enzyme kinetic assay, while the greatest improvement was found when a cyclopropyl group (**1a**) was utilized. Replacement with a cyclohexyl group (**1b**) led to a decrease in performance of the resultant inhibitor, as indicated by increased IC_{50} values (Table 1). These conclusions were further verified via co-crystallization of these inhibitors with M^{pro} and the observation that the cyclopropyl group of **1a** was able to insert deeper into the S2 site of the protease, which may explain the increase in binding affinity (Fig. 2 and Fig. 3A).

Variations in the P3 site of the inhibitor were also made based on our previous work on co-crystallization of M^{pro} with the parent aldehyde GC373 [6]. We noticed that the location in M^{pro} at which the carboxybenzyl (Cbz) group binds (designated as S3) may not be the optimal position. A deeper pocket (designated as S4) can be observed in the vicinity of the Cbz group that may better accommodate the P3 position of the inhibitor, contrasting S3 which appears as a small concave depression pointing towards the surface of M^{pro} (Fig. 2). Therefore, we based further modifications of the P3 position of the inhibitor on two factors: enhancing favorable dipole interactions and inducing strategic conformations of the bound inhibitor.

In order to make improvements at the P3 position based on enhancing dipole interactions, we synthesized a number of structural variants containing polar groups at the benzyl ring of the Cbz group. One variant included a 3-fluorobenzyl group (**1d**) to evaluate the possibility of H-bond formation. Another replaced the benzyl group with a 3-chlorophenylethyl group (**1e**) to evaluate the effect of increased length and flexibility via the introduction of an additional methylene. Selection of a 4-methoxyindole (**1f**) for

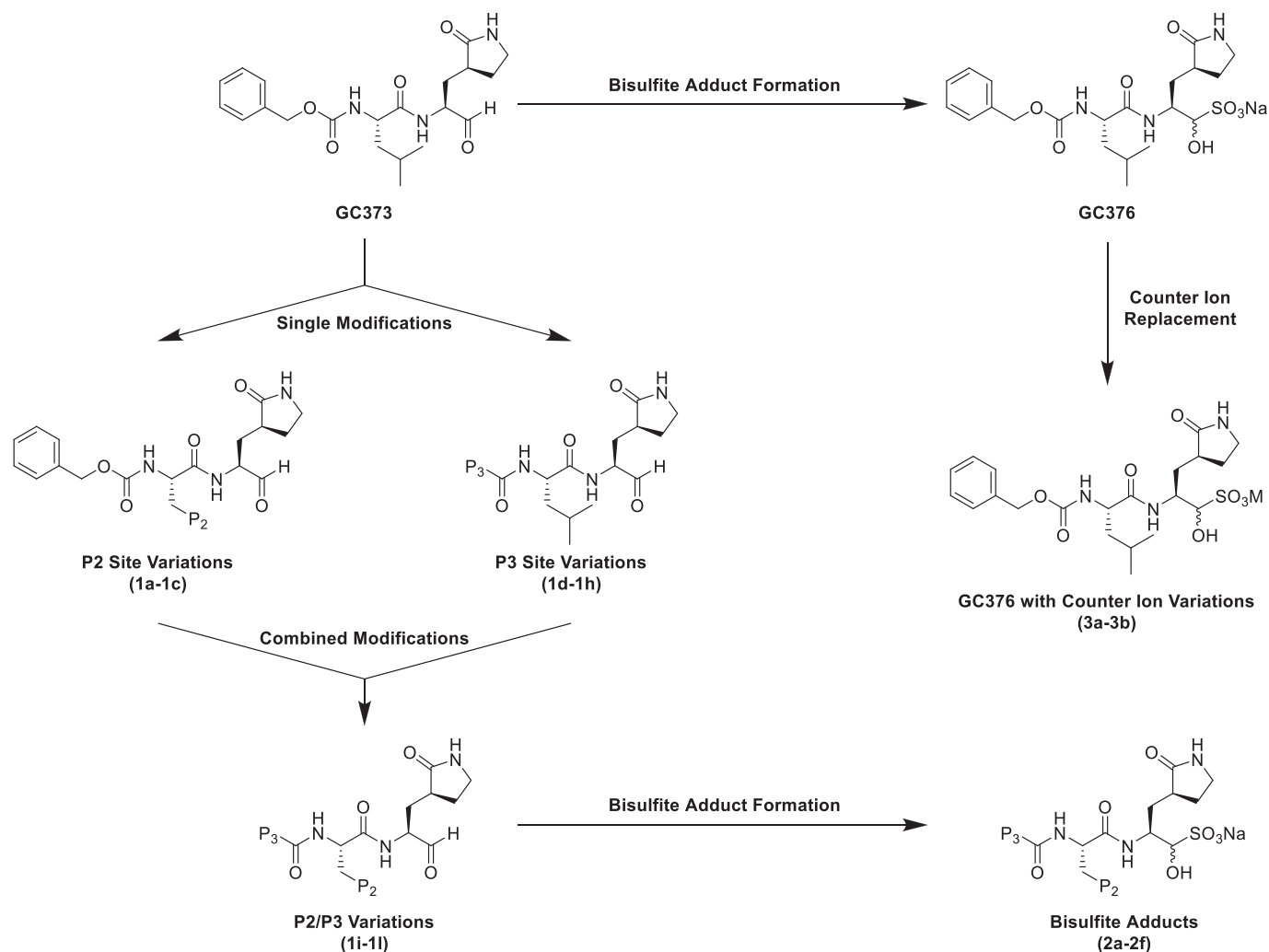


Fig. 1. Developmental workflow of SARS-CoV-2 M^{pro} inhibitors. The process of inhibitor design and modification carried out in this publication is depicted. Evaluation of inhibitors was carried out at each step by FRET studies, crystallography, and viral assays.

evaluation was based on previously reported high affinity of this functionality in binding to SARS-CoV M^{pro} [28]. The second parameter, inducing advantageous conformations, was evaluated *via* stereospecific installation of a methyl group (**1g** and **1h**) at the methylene position of the Cbz group in the parent compound. This methyl group may be able to induce an insertion of the phenyl group into the nearby S4 position of M^{pro}. FRET substrate-enzyme kinetic assays showed that all of these modifications at the P3 position lead to improved IC₅₀ values over GC373, indicating that both of the aforementioned factors played a role in the binding and interactions found at that position (Table 1). The greatest increases in binding affinity resulted from modification of the benzyl group to a 4-methoxyindole variant (**1f**), followed by a 3-fluorobenzyl (**1d**) and 3-chlorophenylethyl variant (**1e**). These were then followed by installation of a methyl group, with the (*S*) absolute configuration (**1g**) outperforming the (*R*) variant (**1h**). As noted in Table 1, **1h** does not exhibit substantially better IC₅₀ values than the parent compound, providing evidence that the absolute stereochemistry at this position plays a modest role in the degree of binding improvement. Taken together, it appears that while both electronic and steric factors play a role, dipole-dipole interactions have a larger effect on improvements in IC₅₀ than that of initial conformation.

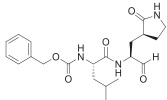
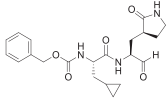
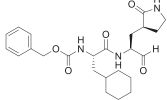
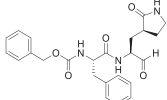
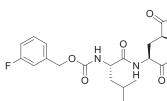
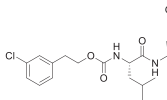
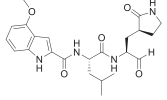
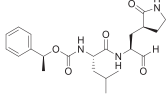
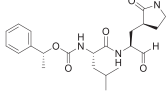
2.2. Combination of most potent P2/P3 modifications

After identifying a number of variations in the P2 and P3 site that lead to improved inhibitor binding to M^{pro}, we combined these modifications to synthesize analogs with potentially improved properties. The optimal modification for the P2 site of the inhibitor was a cyclopropyl moiety, and we therefore combined this with variations at the P3 site. Four additional analogs were obtained (**1i**, **1j**, **1k**, and **1l**), as documented in Table 2 and Fig. S1. Surprisingly, it appeared that there was little or no improvement in IC₅₀ values with these analogs as compared to their singly modified variants (**1d**, **1e**, **1f**, **1g**, Table 1).

In order to improve selectivity, we further transformed a number of these analogs into the bisulfite adduct prodrug versions. In our previous work we found that transformation of the parent aldehyde to the bisulfite adduct resulted in improved IC₅₀ and EC₅₀ values [6], likely a result of increased hydrophilicity and generally improved solubility. The most potent analog from the singular P2 and P3 rounds of modification (**1a** and **1f**) as well as the four combination analogs (**1i**–**1l**) were transformed to the sodium bisulfite adducts in order to see whether this improved binding would take place in this instance as well (Table 3). Interestingly, singularly modified compounds **1a** and **1f** displayed slightly

Table 1

Singly modified aldehyde derivatives of GC373. GC373 and aldehyde derivative structures containing single modifications at either the P2 (**1a–1c**) or P3 (**1d–1h**) positions are shown, along with SARS-CoV-2 M^{Pro} IC₅₀ and SARS-CoV-2 antiviral EC₅₀ values, both with and without co-administration of efflux inhibitor CP-100356 (+CP). Cytotoxicity assays showed CC₅₀ values of >200 μ M for all compounds shown. ND indicates that value was not determined.

Entry	Structure	IC ₅₀ (μ M)	EC ₅₀ (μ M)	EC ₅₀ (μ M) +CP
GC373 [6]		0.40 \pm 0.05	1.5 \pm 0.3	0.32 \pm 0.05
1a (PDB 7LCS)		0.05 \pm 0.01	1.1 \pm 0.1	0.32 \pm 0.09
1b		0.61 \pm 0.15	1.2 \pm 0.4	ND
1c		0.23 \pm 0.10	>10	ND
1d		0.13 \pm 0.04	1.4 \pm 0.5	ND
1e		0.15 \pm 0.05	1.47 \pm 0.8	ND
1f (PDB 7LDL)		0.06 \pm 0.01	0.9 \pm 0.1	0.25 \pm 0.01
1g (PDB 7LCS)		0.27 \pm 0.09	1.1 \pm 0.5	ND
1h		0.35 \pm 0.11	1.4 \pm 0.7	ND

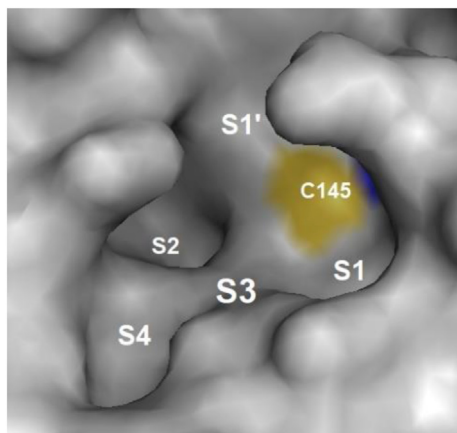


Fig. 2. Binding sites of SARS-CoV-2 M^{Pro} catalytic cleft. The active cysteine-145 residue (C145, yellow) as well as side-pockets S1', S1, S2, S4 and surface depression S3 are highlighted.

increased IC₅₀ values upon transformation to bisulfite adducts **2a** and **2b**. However, doubly modified compounds **2c**, **2d**, **2e**, and **2f** (Table 3, Fig. S2) showed the expected decreases in IC₅₀ values as compared to the parent aldehydes (**1i**, **1j**, **1k**, and **1l**, Table 2). As such, it appears that in many cases, bisulfite adducts of the parent aldehydes indeed lead to improved IC₅₀ values. Of note is that each combination analog as a bisulfite adduct displayed a higher binding affinity for M^{Pro} compared to GC376, ranging from a 2.5–5.0-fold improvement. Testing of variants of GC376 in which the Na⁺ cation was replaced with a K⁺ cation (**3a**) or choline (**3b**) was also conducted, showing very similar IC₅₀ values to that of the parent Na⁺ form (Table 3, Fig. S3), and demonstrating retained effectiveness combined with increased aqueous solubility (discussed below).

2.3. Structural analysis by X-Ray crystallography

In order to better understand interactions of our new inhibitors with the M^{Pro} active site, crystal structures were concurrently

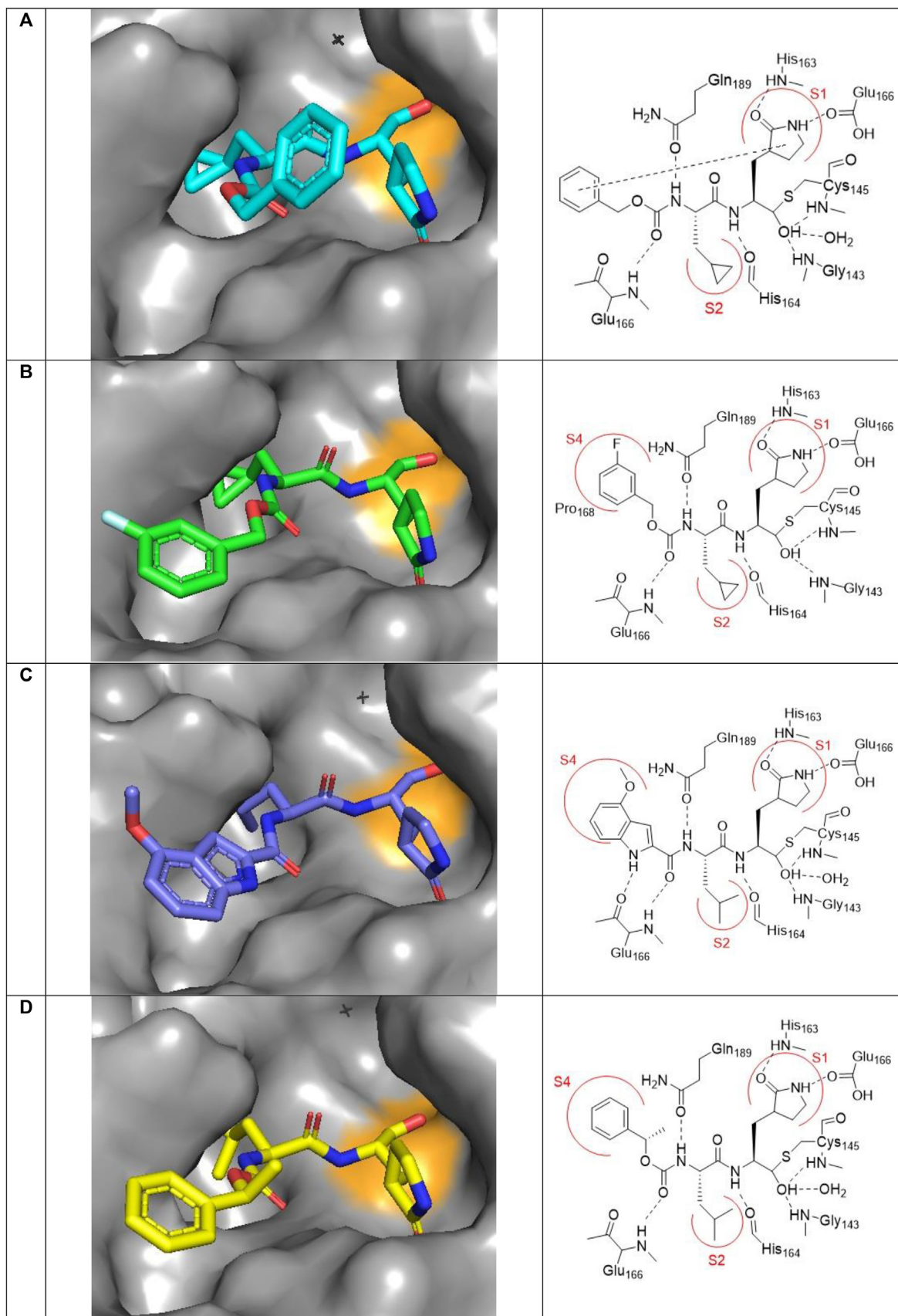


Fig. 3. Crystal structures and schematic depictions of inhibitors bound to SARS-CoV-2 M^{pro}. (A) **1a** bound to the active site of SARS-CoV-2 M^{pro}. The benzyl ring at the P3 position of the inhibitor can be seen interacting with the S3 surface depression, similarly to the binding mode of GC373 (PDB 7LCS). (B) **11** bound to the active site of SARS-CoV-2 M^{pro}. The presence of a fluorine atom at the 3-position on the benzyl ring directs the aromatic moiety into the S4 binding pocket (PDB 7LCO). (C) **1f** bound to the active site of SARS-

obtained throughout the inhibitor development process (Table S1). As previously demonstrated [6], these new structures confirm the formation of a covalent bond between the aldehyde warhead and the active site cysteine of M^{PRO} (Cys145, C–S bond lengths 1.8–2.0 Å). The carbinol hydroxyl maintains favorable hydrogen bonds with the amide NH from both Cys145 and Gly143 of the protease with (**1a**, **1f**, **1g**) or without (**1i**) the coordination of an additional water molecule (Fig. 3A–3D). In accordance with the parent GC373, the lactam carbonyl of the Gln surrogate forms a strong hydrogen bond with the side chain of His163 in the S1 site in all four structures (Fig. 3A–3D). Meanwhile, the lactam NH is also engaged in hydrogen bonds with the side chain oxygen of Glu166 and the backbone oxygen of Phe140, as well as interactions with the N-terminal serine from the other M^{PRO} protomer [26]. Similarly to the Leu-containing analogs **1f** and **1g**, the cyclopropylalanine-bearing compounds **1a** and **1i** (Fig. 3A and B) maintain close C–H $\cdots \pi$ contacts between His41 and the cyclopropyl group, filling the S2 pocket in a more compact fashion than the parent GC373–M^{PRO} structure (PDB 6WTM) where the P2 position does not extend as deeply into the S2 binding pocket [6]. An interesting feature was observed upon examination of the P3 substituent. In the case of a bare Cbz group (i.e. GC373 and **1a**), the P3 residue assumes a tilted conformation pointing towards S3 and the solvent exposed surface of the protease (Fig. 3A). In contrast, substitution of Cbz by a 3-fluorobenzyl group (**1i**, Fig. 3B) or a 4-methoxyindole group (**1f**, Fig. 3C), or by installation of an (S)-methyl group at the benzyl methylene (**1g**, Fig. 3D), forces a relocation of the P3 substituent into the S4 pocket, allowing for additional interactions with that side of the protease. Consequently, in the crystal structure of **1g**, the S–Me group points towards S3 (protease surface), thus defining the attached methylene group as a bifurcation point in inhibitor design (Fig. 3D). Such a space-filling expansion towards both S3 (protease surface) and S4 (binding pocket) has so far not been reported and suggests a promising approach to seal the entrance of the catalytic cleft with a hydrophobic lid. Simultaneously, the N-terminal head group is shown to maintain interactions with Ala188 and Pro168. Of additional note, substitution of the Cbz group with the 4-methoxyindole amide moiety in **1f** (Fig. 3C) leads to a tighter fit in the S4 pocket of M^{PRO} and does not require the coordination of any additional solvent molecules, contrasting a related SARS-CoV-2 M^{PRO} inhibitor structure wherein an indole required the presence of DMSO (PDB 6MOK) [29]. In addition to the NH \cdots O hydrogen bond between the backbone of Glu166 and the terminal inhibitor amide carbonyl O atom, another hydrogen bond between the backbone carbonyl O atom of Glu166 and the indole NH stabilizes the inhibitor in its position.

2.4. Assessment of inhibitory activity and cytotoxicity: plaque reduction and viral assays

While IC₅₀ values provide a drug potency *in vitro* and aid in inhibitor design, EC₅₀ values provide information regarding the drug-potential of the molecule in a living system. We therefore tested our compounds in a viral plaque reduction assay using Vero E6 mammalian cells. In order to assess possible cytotoxic effects, the compounds were also tested using a CellTiter-Glo assay in the same cell line and were found to display therapeutic indices of >200. All inhibitor variants containing lone P2 site modifications (**1a**–**1c**), with the exception of **1c**, exhibited lower EC₅₀ values as compared to the parent GC373, with the cyclopropyl modification

(**1a**) appearing to perform the best. Replicating this, lone P3 site modifications also led to a number of compounds with universally improved EC₅₀ values, with the best performers being **1f** and **1g** (Table 1). Combining the best-performing modifications at each site in the molecule then furnished a number of doubly modified inhibitors (**1i**–**1l**), with two (**1j** and **1k**) demonstrating a further increase in potency and analogous decrease in EC₅₀ values (Table 2). The corresponding sodium bisulfite adducts were derived from the most potent compound from each singly modified group (**2a** and **2b** from **1a** and **1f**, respectively). While **2a** exhibited comparable EC₅₀ values to GC376, indicating similar potential as a drug candidate, **2b** displayed a distinctly higher EC₅₀ value, hinting at possible efflux effects (Table 3). Sodium bisulfite adducts that combined a cyclopropyl group at the P2 position along with P3 substitutions (**2c**–**2f**), had lower EC₅₀ values in two out of four cases, **2c** and **2d**. Based on a recent report in the literature, it was noted that related compounds may be susceptible to cellular efflux, leading to increased EC₅₀ values [30]. In order to determine if this was the case, the EC₅₀ values for a number of our candidates (**1a**, **1f**, **1i**–**1l**, and **2a**–**2f**) were reevaluated in the presence of CP-100356, a P-gp efflux inhibitor (Table 1, Table 2, and Table 3). When administered together with CP-100356, all but three (**1l**, **2b**, and **2f**) of the tested derivatives performed on par or better than the analogous parent GC373 or GC376. Furthermore, the presence of an indole moiety may contribute to efflux, as noted by the comparatively high initial EC₅₀ values of **2b** and **2e** coupled with a significant decrease upon administration of CP-100356, though not to the same extent as reported for related substances [30]. This drop was less significant for the remaining analogs, especially for **2c** and **2d** (Table 3), indicating that while there are some cellular efflux effects present, these new compounds possess the advantage of not requiring the co-administration of efflux inhibitors to be effective, thereby potentially simplifying pharmaceutical development. The results indicate **2c** and **2d** are the most promising inhibitors reported herein (Fig. 4), exhibiting both IC₅₀ and EC₅₀ values that are superior to those of GC376, even in the absence of efflux inhibitors. Replacement of the indole with a 3-fluorobenzyl or 3-chlorophenylethyl group provides the added benefit of increased synthetic yields, contrasting previously described indole-containing inhibitors [2,30], which may facilitate reaction scale-up during process development.

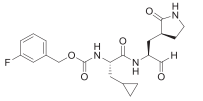
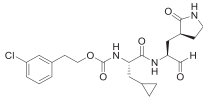
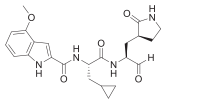
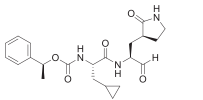
2.5. NMR studies with ¹³C-labelled GC373 and GC376: formation of a dynamic equilibrium of stereoisomeric mixtures in aqueous media

As the mechanism of GC373 and GC376 involves binding of a defined stereoisomer [6], we investigated the properties of GC373 and isomer distribution of both GC373 and GC376 in aqueous media. Versions of GC373 and GC376 having a ¹³C-label at the carbonyl carbon (Fig. S4) were synthesized. An initial HSQC NMR experiment of GC373 in CDCl₃ showed a single prominent signal in the aldehyde region corresponding to the ¹³C-label (Fig. S5A). A second HSQC NMR experiment wherein GC373 was dissolved in aqueous solution (0.5% DMSO-*d*₆ in D₂O) showed that the single aldehyde peak disappeared. It was replaced by 2 signals at ppm values corresponding to formation of two hydrate diastereomers (Fig. S5B) [31], indicating that GC373 epimerizes rapidly and exists almost entirely as the hydrated form in aqueous media [6]. Loss of stereochemical integrity at the α -carbon adjacent to the ¹³C-label in aqueous media is facile for aldehydes of amino acids. Comparison of

CoV-2 M^{PRO}. Substitution of the benzyloxy group with a 4-methoxyindole prompts binding of the P3 portion of the inhibitor to the S4 pocket of the enzyme. This is a result of favorable interactions between the indole nitrogen and the carbonyl of Glu166 as well as that of the methoxy group with the binding pocket itself (PDB 7LDL). (D) **1g** bound to the active site of SARS-CoV-2 M^{PRO}. The phenyl ring of (S)-methyl benzyl group can be seen being directed towards the S4 site of the enzyme *via* the presence of the additional methyl group (PDB 7LCT).

Table 2

Doubly modified aldehyde derivatives of GC373. GC373 and aldehyde derivatives structures containing modifications at both the P2 and P3 positions are shown, along with SARS-CoV-2 M^{Pro} IC₅₀ and SARS-CoV-2 antiviral EC₅₀ values, both with and without co-administration of efflux inhibitor CP-100356 (+CP). Cytotoxicity assays showed CC₅₀ values of >200 μ M for all compounds shown.

Entry	Structure	IC ₅₀ (μ M)	EC ₅₀ (μ M)	EC ₅₀ (μ M) +CP
1i (PDB 7LCO)		0.14 \pm 0.04	1.1 \pm 0.2	0.25 \pm 0.1
1j		0.24 \pm 0.09	0.8 \pm 0.2	0.28 \pm 0.02
1k		0.05 \pm 0.01	0.7 \pm 0.1	0.27 \pm 0.4
1l		0.43 \pm 0.03	2.0 \pm 0.5	1.2 \pm 0.8

peak areas reveals a hydrate diastereomer distribution of ca. 7:3. In the presence of M^{Pro}, there is appearance of an additional peak due to a hemithioacetal formed by binding of a single stereoisomer in the active site of the enzyme. The hydrate diastereomer distribution remained the same as a result of interconversion between the remaining diastereomeric unbound species, suggesting that this equilibrium is dynamic (Fig. S5C). Analogous HSQC NMR experiments with GC376 ¹³C-labelled at the carbonyl carbon also demonstrated a distribution of diastereomers, but only 3 distinct signals were observed at a ratio of 36:46:18 (Fig. S5D). There are 4 different stereochemical permutations possible (Fig. S4), but the range over which their chemical shift values in HSQC spectra may be distributed is limited (Fig. S5E). Hence, it appears that the middle signal is likely an aggregate resulting from spectral overlap of 2 distinct stereochemical species. This study supports the proposal that in aqueous solution, diastereomers of GC373, its hydrate, and GC376, exist in a dynamic stereochemical equilibrium, with only the correct aldehyde isomer binding as a single hemithioacetal in the active site of M^{Pro}.

2.6. Increasing solubility by counter ion variation and investigating aggregation phenomena

In order to help assess the potential of GC376 for administration to humans, a number of solubility experiments were undertaken. We sought to increase the aqueous solubility of GC376 and hypothesized that the cation counterpart to the bisulfite adduct could be replaced with alternative species that exhibited better properties. Potassium and choline were selected as possible candidates owing to larger solvation radii and the generally regarded as safe (GRAS) nature of choline [32]. The potassium and choline counterparts to GC376 (designated as GC376-K (**3a**) and GC376-Cho (**3b**)) were synthesized from GC373 using solutions of potassium or choline bisulfite. Both derivatives demonstrated better solubility in aqueous media, with increases in molar solubility of approximately 30% for GC376-K (**3a**) and over 90% for GC376-Cho (**3b**) compared to GC376. Additionally, GC376-Cho did not appear to form the same turbid solution as GC376 at 50 mM in water (see below). Furthermore, for inhibitors **3a** and **3b**, cellular plaque reduction assays with live virus revealed no significant difference in inhibitory activity as compared to the parent compound GC376

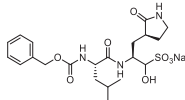
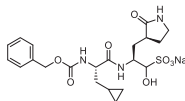
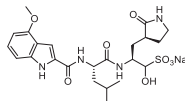
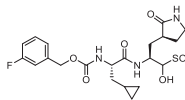
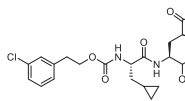
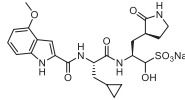
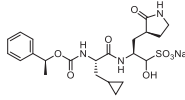
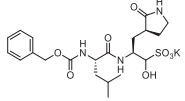
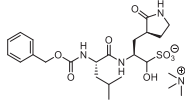
(Table 3), demonstrating that cation replacement is a viable strategy to significantly increase aqueous solubility while retaining activity. This approach represents an attractive general avenue for obtaining more favorable solubility profiles in ion-paired drugs and prodrugs.

It was observed that addition of H₂O or D₂O to powdered GC376 (sodium salt) initially formed clear, transparent solutions at a concentration of ca. 440 mM (Fig. S6A). Further dilution of these transparent solutions resulted in the formation of cloudy colloidal suspensions (Fig. S6B) that eventually became transparent again at sufficiently high dilutions (Fig. S6C). While initially unexpected, this led us to hypothesize that GC376 was forming micelles – a possibility owing to the amphipathic nature of the compound. The bisulfite moiety may function as a polar head group while the largely non-polar peptide backbone and associated side chains may function as a hydrophobic tail, akin in structure to that of a fatty acid. To test this hypothesis, we conducted diffusion-ordered spectroscopy (DOSY) experiments [33] in D₂O at concentrations of 440 mM and 5 mM (Fig. S7), as these concentrations both resulted in the formation of clear solutions. Based on these experiments, a clear difference in diffusion coefficients could be observed, corresponding to 1.2 $\times 10^{-10}$ m²/s at 440 mM and 4.0 $\times 10^{-10}$ m²/s at 5 mM. Accordingly, these diffusion order values correspond to hydrodynamic radii of 20.6 Å and 6.2 Å (41.2 Å and 12.4 Å in diameter) respectively [34] – a distinct difference suggesting the formation of micelles at 440 mM. For comparison, the particle size of extensively studied dodecyl phosphocholine (DPC) micelles in water are noted to be on the order of 64 Å to 72 Å in diameter [35].

Further support of this phenomenon is found when examining the 1D ¹H NMR spectra for these two solutions, with the 440 mM sample producing a spectrum with a number of broad peaks, a known phenomenon in samples exhibiting aggregation (Fig. S8A). Contrasting this, much sharper peaks are observed in the 5 mM sample (Fig. S8B), hinting at dispersed molecules in solution. Expanding upon this, further DOSY experiments were conducted with serially diluted samples of GC376 in D₂O (Table S2). These experiments showed that GC376 possessed a critical micelle concentration of approximately 96.7 mM (Fig. S9A), establishing a new parameter of interest for the development of GC376 and related bisulfite adduct prodrugs. This experiment was repeated with the

Table 3

Bisulfite adduct derivatives of GC373. GC376 and bisulfite adduct derivatives singly (2a, 2b) or doubly (2c–2f) modified at the P2 or P3 positions, or with variations in counter ion (3a, 3b) are shown, along with SARS-CoV-2 MP^{ro} IC_{50} and SARS CoV-2 antiviral EC_{50} values, both with and without co-administration of efflux inhibitor CP-100356 (+CP). Cytotoxicity assays showed CC_{50} values of $>200 \mu M$ for all compounds shown. ND indicates that value was not determined.

Entry	Structure	IC_{50} (μM)	EC_{50} (μM)	EC_{50} (μM) +CP
GC376 [6]		0.19 ± 0.04	0.9 ± 0.2	0.25 ± 0.02
2a		0.08 ± 0.03	0.9 ± 0.3	0.27 ± 0.2
2b		0.07 ± 0.02	1.7 ± 0.3	0.32 ± 0.04
2c		0.07 ± 0.01	0.57 ± 0.07	0.19 ± 0.06
2d		0.08 ± 0.02	0.7 ± 0.2	0.18 ± 0.04
2e		0.04 ± 0.01	1.8 ± 0.4	0.29 ± 0.03
2f		0.05 ± 0.03	1.2 ± 0.2	0.5 ± 0.1
3a		0.20 ± 0.04	0.8 ± 0.3	ND
3b		0.18 ± 0.04	1.2 ± 0.2	ND

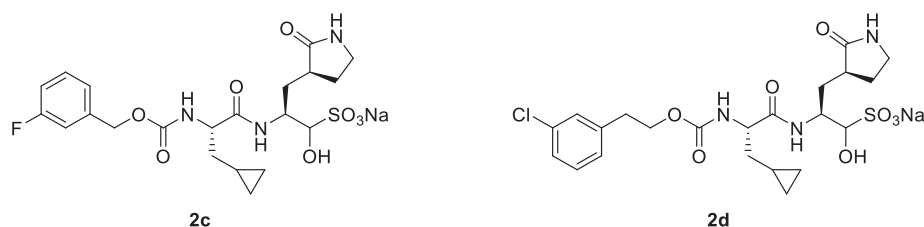


Fig. 4. Key lead compounds identified as improved SARS-CoV-2 MP^{ro} inhibitors. Both structures contain a cyclopropyl group at the P2 position. Differentiation occurs at the P3 position, where **2c** contains a 3-fluorobenzyl group and **2d** contains a 3-chlorophenylethyl group. Both inhibitors show substantially improved potency as demonstrated by IC_{50} and EC_{50} values, both with and without CP-100356, as compared to the parent compound GC376.

choline version of GC376 (GC376-Cho, **3b**), and a corresponding critical micellar concentration of 91.1 mM was observed (Fig. S9B). Previously reported effective dosages of GC376 for felines are established at 5–10 mg/kg/day, twice daily [14]. In humans general volume limits of subcutaneous injection are about 1.5 mL [36]. Administration of a micellar solution of GC376 is a possible method

for circumventing solubility issues and volume limits when considering GC376 for use in human trials. Use of GC376-Cho, with volume requirements as low as 0.11 mL per injection (calculated for a 62 kg human, 5.66 M concentration, 360 mg per injection, MW = 588 g/mol), twice daily, could help to increase patient acceptance. Administration of GC376 or related drugs as a

concentrated micellar or colloid suspension along with the increased solubility resulting from the use of an alternative counterion may allow for significant improvements in the drug profile of these types of peptide-aldehyde inhibitors.

3. Discussion

One of our objectives was to identify new drug candidates for possible treatment of acute COVID-19 based on the antiviral peptide aldehyde GC373 and its bisulfite prodrug GC376. A key goal was to improve on inhibition of the essential viral main protease, SARS-CoV-2 M^{pro}, and on antiviral effects in mammalian cells while maintaining low toxicity [6]. The parent compounds are non-toxic to mammals and effective in curing coronaviral infection in cats [14] and more recently demonstrated, in mouse models [24,25]. A number of new dipeptide derivatives were designed and synthesized with improved IC₅₀ enzyme inhibition and EC₅₀ antiviral values. Inhibitors **2c** and **2d** emerged as key compounds for M^{pro} enzyme inhibition with better IC₅₀ and cellular EC₅₀ values compared to the parent inhibitor GC376. Both **2c** and **2d** are also easier to synthesize in high yield compared to related N-acyl indole derivatives and also out-performs them in EC₅₀ metrics. We note at this point that emerging evidence indicates GC376 and related compounds may exhibit a secondary mechanism of action resulting from the inhibition of cathepsin L, a host-cell protease involved in viral entry [37,38]. Taking this into account, and as a result of Vero E6 cells lacking expression of TMPRSS2 (involved in an alternative viral entry pathway), observed EC₅₀ values may in part be the result of inhibited viral entry, though this remains beyond the scope of this study. X-ray crystallographic studies of four enzyme-inhibitor complexes with SARS-CoV-2 M^{pro} suggest an unexplored avenue for the design of inhibitors with bifurcations at the P3 position to assist in capping the active site. Employment of this strategy may facilitate further development of an additional family of new, potent inhibitors.

Another goal was to examine the properties of GC376 and GC373 in preparation for human clinical trials. Although the prodrug GC376 has worked effectively to treat feline infectious peritonitis (FIP) caused by a coronavirus in cats [14], there are issues that were not reported in detail previously. These include limited aqueous solubility of prodrug GC376 and its tendency to self-aggregate in water, its occurrence as a mixture of stereoisomers, and the tendency of the derived parent aldehyde inhibitor GC373 to isomerize under aqueous conditions. Multidimensional NMR studies (HSQC) of GC373 (aldehyde) and GC376 (bisulfite adduct) with a ¹³C-label at the C-terminal carbons indicate that they form a variety of species in water, some of which are in a dynamic equilibrium with each other. The stereochemically pure GC373 rapidly epimerizes in water due to the acidity of the α -hydrogen adjacent to the aldehyde carbonyl. This then forms a dynamic mixture of two diastereomeric hydrates that predominate in water, but the stereochemically correct aldehyde form, which is one of the equilibrium structures, is selectively captured as a hemithioacetal by the M^{pro} enzyme in the inhibition process. This can be seen as a single species in the enzyme active site both by NMR spectroscopy and protein X-ray crystallography. Formation of bisulfite GC376, which is done under aqueous conditions, can proceed from either the *re* or *si* faces of the carbonyl for each of the aldehyde diastereomers. This nominally results in formation of four diastereomeric bisulfite adducts, with at least three being observed by HSQC NMR (chemical shifts for two appear to overlap). However, in water the bisulfite adducts readily revert to the aldehyde forms, which being readily epimerized, provide the active inhibitory stereoisomer.

In humans, weight-adjusted dosage for subcutaneous injections of GC376 is higher than in cats, and therefore aqueous solubility

and injection volume is an important issue. Our work has revealed previously unreported self-aggregation and colloidal properties of the compound. High concentrations (440 mM) of GC376 in water form a clear, viscous solution. Upon dilution, the solution becomes a cloudy colloidal dispersion and ultimately becomes fully homogeneous at sufficiently low concentrations (5 mM). Replacement of the sodium counterion of GC376 with potassium or choline enhances solubility considerably. As the more potent analogs that were synthesized for enzyme inhibition studies are structurally related, they are likely to share many of these physical properties. We believe that micellar administration of bisulfite adducts in combination with cation replacement could enable the pharmaceutical development of a large number of inhibitors previously limited by solubility issues. In conclusion, a number of alternative compounds with more favorable drug-like properties were designed and tested with desirable therapeutic indices of over 200. The results of this study present insights and tools for drug development based on cysteine protease inhibitors with implications not limited to just SARS-CoV-2.

4. Materials and methods

4.1. FRET peptide substrate synthesis

The FRET substrate Abz-SVTLSQSG-Y(NO₂)-R used was synthesized according to the methods previously described in literature [6]. Characterization data was in accordance as described.

4.2. Isolation and purification of SARS-CoV-2 M^{pro}

Pure SARS-CoV-2 M^{pro} was obtained as described previously and confirmed according to established data [6].

4.3. Inhibition assay and determination of IC₅₀ values

IC₅₀ values for each inhibitor tested was determined via the methods described previously in literature [6].

4.4. Crystallization of M^{pro}

The purified SARS-CoV-2 M^{pro} was dialyzed against buffer containing 10 mM NaCl and 5 mM Tris HCl pH 8.0 overnight at 4 °C. Protein was concentrated with a Millipore centrifugal filter (10 kDa MW cutoff) to a concentration of 8 mg/mL. Protein was incubated with 5 mM excess of inhibitor at 4 °C for 1 h prior to crystallization. The SARS-CoV-2 M^{pro}, the protein was subjected to the JCSG plus and PACT crystallization screen (Molecular Dimensions), with hits identified in several conditions for all inhibitors. Best crystals were observed with hanging drop trays at room temperature at a ratio of 1:1 with mother liquor 0.2 M Sodium chloride, 0.1 M HEPES pH 7.0, 20% w/v PEG 6000. Prior to freezing, crystals were incubated with 19% glycerol as a cryoprotectant. Data collection was take place at SSRL, beamline 12-2 with Blu-Ice using the Web-Ice interface and Canadian Light Source beamline 08B1-1 using MxDC.

4.5. Diffraction data collection, phase determination, model building, and refinement

X-ray diffraction data sets for SARS-CoV-2 M^{pro} and inhibitor complex were collected at 100 K in a cold nitrogen stream using beamlines at 12-2 at Stanford Synchrotron Radiation Lightsource (SSRL) California, USA, of wavelength 0.97946, equipped with Dectris PILATUS 6 M detector and Canadian light Source, CLSI BEAMLINE 08B1-1 coupled with PILUUS 6 M. More than 80 data

sets were collected for all the five inhibitors, all of them processed and the best ones selected based on data statistics. XDS and Scala were used for processing of the data sets. The diffraction data set of the Lig124 (XU4) SARS-CoV-2 M^{pro} was processed at a resolution of 1.93 Å, in an orthorhombic space group P2₁2₁2 (Supplementary Table 1). For the complex of SARS-CoV-2 M^{pro} with ligand 180 (XTJ), the data set collected, was processed at a resolution of 1.90 Å in a space group C2, Ligand 182 (XV4) processed at resolution of 2.0 Å in a monoclinic space group P1. The data set collected for Lig128 (XTP) at resolution 1.85 Å, processed in a space group C2. The data set collected for Lig132 (XTM) in an orthorhombic space group P2₁2₁2₁ refined at resolution 1.95 Å. (Table S1). All the five structures were determined by molecular replacement with the crystal structure of the free enzyme of the SARS-CoV-2 M^{pro} (PDB entry 6WTM) [6] as a search model, using the Phaser program from Phenix, version v1.18.1–3855). Ligand was fit using Coot manually for all the inhibitors in the density of pre-calculated map from Phenix refinement. Refinement of all the structures was performed with phenix.refine in Phenix software. The structure refinement yielded final R_{work} and R_{free} of reasonable values. Statistics of diffraction, data processing and model refinement are given in the supplementary materials (Table S1). The model was inspected with Ramachandran plots and all show good stereochemistry. Final models displayed using PyMOL molecular graphics software (Version 2.0 Schrödinger, LLC).

4.6. Plaque reduction assay and EC₅₀ determination

Plaque reduction assay for EC₅₀ determination was carried out with live virus in Vero cells using the methods that we have previously described [6].

4.7. Evaluation of inhibitor cytotoxicity

Cytotoxicity of inhibitors was determined using the methods that we have previously described [6].

4.8. Population distribution studies

¹³C-labelled substrate was prepared in accordance with procedures documented in the supplemental materials. NMR samples of GC373 were prepared by dissolving the sample in CDCl₃ or in the case of D₂O, as a solution in DMSO-*d*₆ that was subsequently diluted to a final concentration of 1% DMSO-*d*₆ in D₂O. Preparation of GC376 samples omitted the use of DMSO-*d*₆ as a co-solvent. Additional information and protocols for samples containing M^{pro} enzyme can be found previously documented in literature [6]. Experiments were executed on a 700 MHz Agilent VNMR spectrometer equipped with a cryo-cooled HCN triple resonance Z-gradient probe.

4.9. Solubility studies

Solubility studies were carried out by depositing 10 mg of bisulfite prodrug (differing in cation – Na, K, or choline) in a small conical vial and sequentially adding H₂O in 0.5 µL increments at 25 °C. These mixtures were then alternately vortexed using a desktop instrument (30 s) and sonicated in a water bath (30 s) 3x each. The mixtures were then observed to see if and solids remained. Additional volumes of H₂O (in 0.5 µL increments) were added followed by vortexing and sonication steps until a clear, transparent mixture was obtained. Back calculation then allowed for determination of upper solubility limits for each variant of bisulfite salt.

4.10. DOSY experiments

Diffusion Ordered Spectroscopy (DOSY) measurements were performed on a 600 MHz four-channel Varian VNMR spectrometer equipped with a HCN Z-gradient probe using OpenVNMRJ 2.1A as the acquisition and processing software. The Oneshot45 DOSY pulse sequence [39,40] was used for all diffusion measurements. All experiments were done at 27 °C. The 90° pulse was optimized for each sample using a simple pulse acquire NMR experiment with presaturation of the residual HOD during the relaxation delay. The diffusion delay was optimized for each sample using the Oneshot45 pulse sequence using 5 different pulsed field gradient strengths from 2.4 G/cm to 59.5 G/cm. Based on the optimized diffusion delay, for GC376 and 3b diffusion delays of 50 ms–200 ms were used, the final DOSY experiment was acquired using 15 different pulsed field gradient strengths from 2 G/cm to 59.5 G/cm with 12 scans for each value of gradient strength. The DOSY data were base line corrected and then processed using a two component fit, were corrected for non-uniform pulsed field gradient shapes and plotted using the DOSY module in OpenVNMRJ 2.1A.

Funding

These investigations were supported by the Natural Sciences and Engineering Research Council of Canada (NSERC) and the Canadian Institutes of Health Research (COVID-19 SOF-549297-2019 and VR3-172655).

Author contributions

W.V., C.F., J.A.N. and J.C.V. contributed to inhibitor design. W.V. and C.F. contributed to inhibitor synthesis. T.L. and K.W. contributed to FRET substrate synthesis. C.F. contributed to FRET assay studies. W.V. and C.F. contributed to solubility studies. W.V. contributed to NMR studies. C.F. and M.J.v.B. contributed to purified protein. M.B.K. and M.J.L. contributed to protein crystallography. M.A.J., H.A.S., J.A.S., and D.L.T. contributed to viral and toxicity studies. W.V. wrote the initial draft. All authors read and approved the manuscript.

Declaration of competing interest

The authors declare no competing interests.

Acknowledgments

General: The authors thank Mark Miskolzie and Ryan McKay for help with NMR analyses and assistance in DOSY experiments. We are grateful to Randy Whittall, Jing Zheng, Angelina Morales-Izquierdo, and Béla Reiz for assistance with mass spectrometry. We also thank Wayne Moffatt and Jennifer Jones for assistance in compound characterization. Helpful discussions with David Bruyette (Anivive Lifesciences Inc., Long Beach CA) are gratefully acknowledged.

Appendix A. Supplementary data

Supplementary data to this article can be found online at <https://doi.org/10.1016/j.ejmech.2021.113584>.

References

- [1] H. Wang, X. Li, T. Li, S. Zhang, L. Wang, X. Wu, J. Liu, The genetic sequence, origin, and diagnosis of SARS-CoV-2, *Eur. J. Clin. Microbiol. Infect. Dis.* (2020) 1–7, <https://doi.org/10.1007/s10096-020-03899-4>.
- [2] L. Zhang, D. Lin, X. Sun, U. Curth, C. Drosten, L. Sauerhering, S. Becker, K. Rox, R. Hilgenfeld, Crystal structure of SARS-CoV-2 main protease provides a basis

- for design of improved α -ketoamide inhibitors, *Science* 368 (2020) 409–412.
- [3] COVID-19 map, Johns Hopkins coronavirus resource center (n.d.), <https://coronavirus.jhu.edu/map.html>. (Accessed 11 December 2020).
- [4] A contemporary view of coronavirus transcription [J. Virol., (n.d.). <https://jvi.asm.org/content/81/1/20> (accessed February 6, 2021).
- [5] T. Pillaiyar, M. Manickam, V. Namasivayam, Y. Hayashi, S.-H. Jung, An overview of severe acute respiratory syndrome–coronavirus (SARS-CoV) 3CL protease inhibitors: peptidomimetics and small molecule chemotherapy, *J. Med. Chem.* 59 (2016) 6595–6628, <https://doi.org/10.1021/acs.jmedchem.5b01461>.
- [6] W. Vuong, M.B. Khan, C. Fischer, E. Arutyunova, T. Lamer, J. Shields, H.A. Saffran, R.T. McKay, M.J. van Belkum, M.A. Joyce, H.S. Young, D.L. Tyrrell, J.C. Vederas, M.J. Lemieux, Feline coronavirus drug inhibits the main protease of SARS-CoV-2 and blocks virus replication, *Nat. Commun.* 11 (2020) 4282, <https://doi.org/10.1038/s41467-020-18096-2>.
- [7] H.-H. Otto, T. Schirmeister, Cysteine proteases and their inhibitors, *Chem. Rev.* 97 (1997) 133–172, <https://doi.org/10.1021/cr950025u>.
- [8] M. Drag, G.S. Salvesen, Emerging principles in protease-based drug discovery, *Nat. Rev. Drug Discov.* 9 (2010) 690–701, <https://doi.org/10.1038/nrd3053>.
- [9] A.K. Patick, S.L. Binford, M.A. Brothers, R.L. Jackson, C.E. Ford, M.D. Diem, F. Maldonado, P.S. Dragovich, R. Zhou, T.J. Prins, S.A. Fuhrman, J.W. Meador, L.S. Zalman, D.A. Matthews, S.T. Worland, In vitro antiviral activity of AG7088, a potent inhibitor of human rhinovirus 3C protease, *Antimicrob. Agents Chemother.* 43 (1999) 2444–2450, <https://doi.org/10.1128/AAC.43.10.2444>.
- [10] J. Rocha-Pereira, M.S.J. Nascimento, Q. Ma, R. Hilgenfeld, J. Neyts, D. Jochmans, The enterovirus protease inhibitor rupintrivir exerts cross-genotypic antinorovirus activity and clears cells from the norovirus replicon, *Antimicrob. Agents Chemother.* 58 (2014) 4675–4681.
- [11] J.O. Westerik, R. Wolfenden, Aldehydes as inhibitors of papain, *J. Biol. Chem.* 247 (1972) 8195–8197.
- [12] B.A. Malcolm, C. Lowe, S. Shechosky, R.T. McKay, C.C. Yang, V.J. Shah, R.J. Simon, J.C. Vederas, D.V. Santi, Peptide aldehyde inhibitors of hepatitis A virus 3C proteinase, *Biochemistry* 34 (1995) 8172–8179, <https://doi.org/10.1021/bi00025a024>.
- [13] S.R. Mandadapu, M.R. Gunnam, K.-C. Tiew, R.A.Z. Uy, A.M. Prior, K.R. Alliston, D.H. Hua, Y. Kim, K.-O. Chang, W.C. Groutas, Inhibition of norovirus 3CL protease by bisulfite adducts of transition state inhibitors, *Bioorg. Med. Chem. Lett.* 23 (2013) 62–65, <https://doi.org/10.1016/j.bmcl.2012.11.026>.
- [14] Y. Kim, H. Liu, A.C. Galasiti Kankanamalage, S. Weerasekara, D.H. Hua, W.C. Groutas, K.-O. Chang, N.C. Pedersen, Reversal of the progression of fatal coronavirus infection in cats by a broad-spectrum coronavirus protease inhibitor, *PLoS Pathog.* 12 (2016), e1005531, <https://doi.org/10.1371/journal.ppat.1005531>.
- [15] K.D. Perera, A.C. Galasiti Kankanamalage, A.D. Rathnayake, A. Honeyfield, W. Groutas, K.-O. Chang, Y. Kim, Protease inhibitors broadly effective against feline, ferret and mink coronaviruses, *Antivir. Res.* 160 (2018) 79–86, <https://doi.org/10.1016/j.antiviral.2018.10.015>.
- [16] Y. Kim, S. Lovell, K.-C. Tiew, S.R. Mandadapu, K.R. Alliston, K.P. Battaile, W.C. Groutas, K.-O. Chang, Broad-spectrum antivirals against 3C or 3C-like proteases of picornaviruses, noroviruses, and coronaviruses, *J. Virol.* 86 (2012) 11754–11762, <https://doi.org/10.1128/JVI.01348-12>.
- [17] M.D. Sacco, C. Ma, P. Lagarias, A. Gao, J.A. Townsend, X. Meng, P. Dube, X. Zhang, Y. Hu, N. Kitamura, B. Hurst, B. Tarbet, M.T. Marty, A. Kolocouris, Y. Xiang, Y. Chen, J. Wang, Structure and inhibition of the SARS-CoV-2 main protease reveal strategy for developing dual inhibitors against Mpro and cathepsin L, *Science Advances* 6 (2020), eabe0751, <https://doi.org/10.1126/sciadv.abe0751>.
- [18] L. Fu, F. Ye, Y. Feng, F. Yu, Q. Wang, Y. Wu, C. Zhao, H. Sun, B. Huang, P. Niu, H. Song, Y. Shi, X. Li, W. Tan, J. Qi, G.F. Gao, Both Boceprevir and GC376 efficaciously inhibit SARS-CoV-2 by targeting its main protease, *Nat. Commun.* 11 (2020) 4417, <https://doi.org/10.1038/s41467-020-18233-x>.
- [19] C. Ma, M.D. Sacco, B. Hurst, J.A. Townsend, Y. Hu, T. Szeto, X. Zhang, B. Tarbet, M.T. Marty, Y. Chen, J. Wang, Boceprevir, GC-376, and calpain inhibitors II, XII inhibit SARS-CoV-2 viral replication by targeting the viral main protease, *Cell Res.* (2020) 1–15, <https://doi.org/10.1038/s41422-020-0356-z>.
- [20] S. Iketani, F. Forouhar, H. Liu, S.J. Hong, F.-Y. Lin, M.S. Nair, A. Zask, Y. Huang, L. Xing, B.R. Stockwell, A. Chavez, D.D. Ho, Lead compounds for the development of SARS-CoV-2 3CL protease inhibitors, *BioRxiv* (2020), <https://doi.org/10.1101/2020.08.03.235291>.
- [21] H.-C. Hung, Y.-Y. Ke, S.Y. Huang, P.-N. Huang, Y.-A. Kung, T.-Y. Chang, K.-J. Yen, T.-T. Peng, S.-E. Chang, C.-T. Huang, Y.-R. Tsai, S.-H. Wu, S.-J. Lee, J.-H. Lin, B.-S. Liu, W.-C. Sung, S.-R. Shih, C.-T. Chen, J.T.-A. Hsu, Discovery of M Protease inhibitors encoded by SARS-CoV-2, *Antimicrob. Agents Chemother.* 64 (2020), <https://doi.org/10.1128/AAC.00872-20>.
- [22] Y.-C. Wang, W.-H. Yang, C.-S. Yang, M.-H. Hou, C.-L. Tsai, Y.-Z. Chou, M.-C. Hung, Y. Chen, Structural basis of SARS-CoV-2 main protease inhibition by a broad-spectrum anti-coronaviral drug, *Am J Cancer Res* 10 (2020) 2535–2545.
- [23] J. Qiao, Y.-S. Li, R. Zeng, F.-L. Liu, R.-H. Luo, C. Huang, Y.-F. Wang, J. Zhang, B. Quan, C. Shen, X. Mao, X. Liu, W. Sun, W. Yang, X. Ni, K. Wang, L. Xu, Z.-L. Duan, Q.-C. Zou, H.-L. Zhang, W. Qu, Y.-H.-P. Long, M.-H. Li, R.-C. Yang, X. Liu, J. You, Y. Zhou, R. Yao, W.-P. Li, J.-M. Liu, P. Chen, Y. Liu, G.-F. Lin, X. Yang, J. Zou, L. Li, Y. Hu, G.-W. Lu, W.-M. Li, Y.-Q. Wei, Y.-T. Zheng, J. Lei, S. Yang, SARS-CoV-2 Mpro inhibitors with antiviral activity in a transgenic mouse model, *Science* 371 (2021) 1374–1378, <https://doi.org/10.1126/science.abbf1611>.
- [24] C.J. Cáceres, S. Cardenas-Garcia, S. Carnaccini, B. Seibert, D.S. Rajao, J. Wang, D.R. Perez, Efficacy of GC-376 against SARS-CoV-2 virus infection in the K18 hACE2 transgenic mouse model, *BioRxiv* (2021), <https://doi.org/10.1101/2021.01.27.428428>, 2021.01.27.428428.
- [25] Y. Shi, L. Shuai, Z. Wen, C. Wang, Y. Yan, Z. Jiao, F. Guo, Z.F. Fu, H. Chen, Z. Bu, G. Peng, The preclinical inhibitor GS441524 in combination with GC376 efficaciously inhibited the proliferation of SARS-CoV-2 in the mouse respiratory tract, *Emerg. Microb. Infect.* 10 (2021) 481–492, <https://doi.org/10.1080/22221751.2021.1899770>.
- [26] E. Arutyunova, M.B. Khan, C. Fischer, J. Lu, T. Lamer, W. Vuong, M.J. van Belkum, R.T. McKay, D.L. Tyrrell, J.C. Vederas, H.S. Young, M.J. Lemieux, N-Terminal finger stabilizes the reversible feline drug GC376 in SARS-CoV-2 Mpro, *BioRxiv* (2021), <https://doi.org/10.1101/2021.02.16.431021>, 2021.02.16.431021.
- [27] R.L. Hoffman, R.S. Kania, M.A. Brothers, J.F. Davies, R.A. Ferre, K.S. Gajiwala, M. He, R.J. Hogan, K. Kozminski, L.Y. Li, J.W. Lockner, J. Lou, M.T. Marra, L.J. Mitchell, B.W. Murray, J.A. Nieman, S. Noell, S.P. Planken, T. Rowe, K. Ryan, G.J. Smith, J.E. Solowiej, C.M. Steppan, B. Taggart, Discovery of ketone-based covalent inhibitors of coronavirus 3CL proteases for the potential therapeutic treatment of COVID-19, *J. Med. Chem.* 63 (2020) 12725–12747, <https://doi.org/10.1021/acs.jmedchem.0c01063>.
- [28] P. Thanigaimalai, S. Konno, T. Yamamoto, Y. Koiwai, A. Taguchi, K. Takayama, F. Yakushiji, K. Akaji, S.-E. Chen, A. Naser-Tavakolian, A. Schön, E. Freire, Y. Hayashi, Development of potent dipeptide-type SARS-CoV 3CL protease inhibitors with novel P3 scaffolds: design, synthesis, biological evaluation, and docking studies, *Eur. J. Med. Chem.* 68 (2013) 372–384, <https://doi.org/10.1016/j.ejmech.2013.07.037>.
- [29] W. Dai, B. Zhang, X.-M. Jiang, H. Su, J. Li, Y. Zhao, X. Xie, Z. Jin, J. Peng, F. Liu, C. Li, Y. Li, F. Bai, H. Wang, X. Cheng, X. Cen, S. Hu, X. Yang, J. Wang, X. Liu, G. Xiao, H. Jiang, Z. Rao, L.-K. Zhang, Y. Xu, H. Yang, H. Liu, Structure-based design of antiviral drug candidates targeting the SARS-CoV-2 main protease, *Science* 368 (2020) 1331–1335, <https://doi.org/10.1126/science.abb4489>.
- [30] Discovery of a novel inhibitor of coronavirus 3CL protease as a clinical candidate for the potential treatment of COVID-19 | *bioRxiv*, (n.d.). <https://www.biorxiv.org/content/10.1101/2020.09.12.293498v2> (accessed December 11, 2020).
- [31] B.A. Malcolm, C. Lowe, S. Shechosky, R.T. McKay, C.C. Yang, V.J. Shah, R.J. Simon, J.C. Vederas, D.V. Smith, Peptide aldehyde inhibitors of hepatitis A virus 3C proteinase, *Biochemistry* 34 (1995) 8172–8179, <https://doi.org/10.1021/bi00025a024>.
- [32] Cfr - code of federal regulations title 21 (n.d.), <https://www.accessdata.fda.gov/scripts/cdrh/cfdocs/cfcr/CFRSearch.cfm?fr=182.8252>. (Accessed 12 December 2020).
- [33] Y. Bakkour, V. Darcos, S. Li, J. Coudane, Diffusion ordered spectroscopy (DOSY) as a powerful tool for amphiphilic block copolymer characterization and for critical micelle concentration (CMC) determination, *Polym. Chem.* 3 (2012) 2006–2010, <https://doi.org/10.1039/c2py20054f>.
- [34] L. Costigliola, D.M. Heyes, T.B. Schröder, J.C. Dyre, Revisiting the Stokes-Einstein relation without a hydrodynamic diameter, *J. Chem. Phys.* 150 (2019), 021101, <https://doi.org/10.1063/1.5080662>.
- [35] E. Sikorska, D. Wyrzykowski, K. Szutkowski, K. Greber, E.A. Lubecka, I. Zhukov, Thermodynamics, size, and dynamics of zwitterionic dodecylphosphocholine and anionic sodium dodecyl sulfate mixed micelles, *J. Therm. Anal. Calorim.* 123 (2016) 511–523, <https://doi.org/10.1007/s10973-015-4918-0>.
- [36] R. Mathaes, A. Koulou, S. Joerg, H.-C. Mahler, Subcutaneous injection volume of biopharmaceuticals—pushing the boundaries, *J. PharmSci* 105 (2016) 2255–2259, <https://doi.org/10.1016/j.xphs.2016.05.029>.
- [37] K. Steuten, H. Kim, J.C. Widen, B.M. Babin, O. Onguka, S. Lovell, O. Bolgi, B. Cerikan, C.J. Neufeldt, M. Cortese, R.K. Muir, J.M. Bennett, R. Geiss-Friedlander, C. Peters, R. Bartenschlager, M. Bogoy, Challenges for targeting SARS-CoV-2 proteases as a therapeutic strategy for COVID-19, *ACS Infect. Dis.* (2021), <https://doi.org/10.1021/acsinfecdis.0c00815>.
- [38] Y. Hu, C. Ma, T. Szeto, B. Hurst, B. Tarbet, J. Wang, Boceprevir, calpain inhibitors II and XII, and GC-376 have broad-spectrum antiviral activity against coronaviruses, *ACS Infect. Dis.* 7 (2021) 586–597, <https://doi.org/10.1021/acsinfecdis.0c00761>.
- [39] M.D. Pelta, G.A. Morris, M.J. Stchedroff, S.J. Hammond, A one-shot sequence for high-resolution diffusion-ordered spectroscopy, *Magn. Reson. Chem.* 40 (2002) S147–S152, <https://doi.org/10.1002/mrc.1107>.
- [40] A. Botana, J.A. Aguilar, M. Nilsson, G.A. Morris, J-modulation effects in DOSY experiments and their suppression: the Oneshot45 experiment, *J. Magn. Reson.* 208 (2011) 270–278, <https://doi.org/10.1016/j.jmr.2010.11.012>.